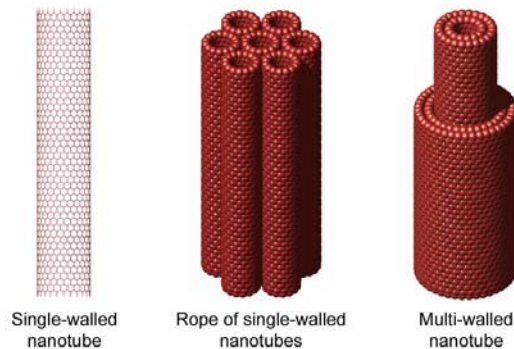# CARBON NANOTUBES FOR SPACE PHOTOVOLTAIC APPLICATIONS

Brian J. Landi, Patrick L. Denno, Roberta A. DiLeo, William VanDerveer, and Ryne P. Raffaelle
Rochester Institute of Technology, Rochester, NY

Harry Efstathiadis and Pradeep Haldar
University at Albany, Albany, NY

Introduction

Carbon nanotubes (CNTs) can be envisioned as an individual graphene sheet rolled into a seamless cylinder (single-walled, SWNT), or concentric sheets as in the case of a multi-walled carbon nanotube (MWNT) (1). The role-up vector will determine the hexagonal arrangement and "chirality" of the graphene sheet, which will establish the nanotube to be metallic or semiconducting. The optoelectronic properties will depend directly on this chiral angle and the diameter of the SWNT, with semiconductor types exhibiting a band gap energy (2). Characteristic of MWNTs are the concentric graphene layers spaced 0.34 nm apart, with diameters from 10-200 nm and lengths up to hundreds of microns (2). In the case of SWNTs, the diameters range from 0.4 – 2 nm and lengths have been reported up to 1.5 cm (3). SWNTs have the distinguishable property of "bundling" together due to van der Waal's attractions to form "ropes." A comparison of these different structural types is shown in Figure 1.

Single-walled nanotube   Rope of single-walled nanotubes   Multi-walled nanotube

Figure 1. Schematic representation of carbon nanotube structures (4).

The use of SWNTS in space photovoltaic (PV) applications is attractive for a variety of reasons. Carbon nanotubes as a class of materials exhibit unprecedented optical, electrical, mechanical properties, with the added benefit of being nanoscale in size which fosters ideal interaction in nanomaterial-based devices like polymeric solar cells. The optical bandgap of semiconducting SWNTs can be varied from ~ 0.4 – 1.5 eV, with this property being inversely proportional to the nanotube diameter. Recent work at GE Global Research has shown where a single nanotube device can behave as an "ideal" pn diode (5). The SWNT was bridged over a SiO_2 channel between Mo contacts and exhibited an ideality factor of 1, based on a fit of the current-voltage data using the diode equation. The measured PV efficiency under a 0.8 eV monochromatic illumination showed a power conversion efficiency of 0.2 %. However, the projected efficiency of these junctions is estimated to be > 5 %, especially when one considers the enhanced absorption (from nanotubes whose bandgap is tailored to illumination) and electromagnetic coupling in a network of nanotubes.

The high conductivity of carbon nanotubes (electrical = 10^4 S/cm (6) and thermal = 6600 W/mK for a (10,10) SWNT (7)) represents another potential contribution to space PV for use as electrical interconnects for arrays or as enhanced solar cell contacts. Other beneficial properties of SWNTs relevant to space photovoltaics include composite reinforcement and thermal management. SWNTs have shown promise in the development of polymer composites with enhanced mechanical strength by load transfer from polymer or epoxy matrices to the nanotubes

(8). Tensile strengths for SWNTs have been estimated to equal ~20 GPa (9), while the Young's modulus measured by atomic force microscopy is ~1 TPa (10). This high Young's modulus and strength-to-weight ratio could help provide much needed mechanical stability in large area thin-film arrays.

The dimensions of carbon nanotubes give rise to extraordinary aspect ratios (length/diameter), which is extremely advantageous for establishing low percolation thresholds in polymer or ceramic composites. The percolation pathways allow for high carrier mobility, while the extremely high surface area, ~1600 m^2/g reported for purified SWNTs (11), offers a tremendous opportunity for exciton dissociation in an optically excited polymer. The utility of SWNTs in a conducting polymer for photovoltaic devices was established in 2002, with arc-generated SWNT- poly(3-octylthiophene)-(P3OT) composites (12). Their results showed a diode response for devices constructed in the sandwich formation, containing the composite film between an indium-tin-oxide (ITO) front contact and aluminum back contact (see Figure 2). Their results and ours (13) have shown relatively high open-circuit voltages (V_{OC}) for SWNT-P3OT devices (~ 1 V), albeit the overall efficiencies are still below 1 %. The V_{OC} in these devices is predicted to result from the energy level differences in the highest occupied molecular orbital (HOMO) level of the polymer and the electron affinity of the carbon nanotubes. In addition, the semiconducting SWNTs have the inherent ability to absorb bandgap-specific light to produce free carriers (13). These properties, as shown in Figure 2, result in a tremendous potential for higher efficiency polymer cells using carbon nanotubes.   However, given the applications of carbon nanotubes in space PV, there are also real challenges present towards realizing these advancements. In this paper, we highlight several critical areas in carbon nanotube development: material synthesis, purity assessment, bandgap engineering, and polymer solar cell approaches; which can evolve this emerging technology into more efficient PV devices.
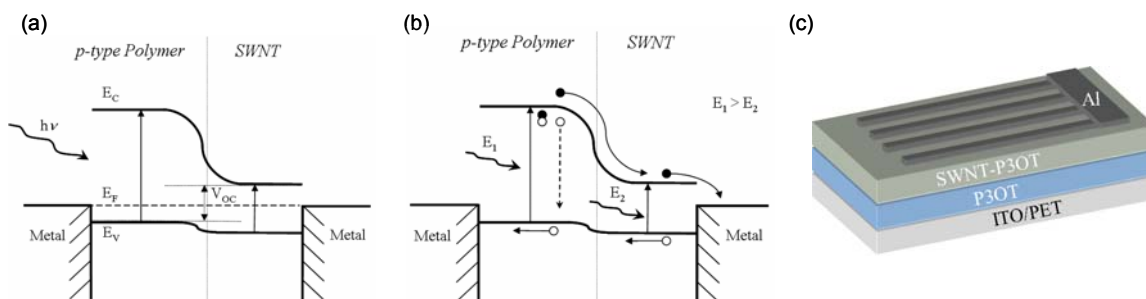

Figure 2. (a) energy level diagram for SWNT-Polymer solar cell depicting the nanomaterial junction and (b) charge transfer process. (c) schematic representation of a typical SWNT-Polymer solar cell.

Experimental

The synthesis of carbon nanotubes can be from a wide variety of different methods that involve the catalytic decomposition of a carbon containing gas or solid. Some of the most common techniques are chemical vapor deposition, arc-discharge, and laser vaporization synthesis (2,14). The synthesis conditions (temperature, pressure, carrier gas, etc), metal catalyst type (most commonly iron, nickel, cobalt or yttrium), and carbon source (graphite or hydrocarbon) have all been shown to influence the properties of the resulting carbon nanotubes (2,15,16). In the present work, laser-synthesized SWNTs are produced using an Alexandrite laser (755 nm) which rasters over the surface of a Ni/Co-doped graphite target at an average power density of 100 W/cm^2. The reactor temperature is constant at 1150 °C under flowing $Ar_{(g)}$ and 700 torr (17,18). A schematic summarizing the process is shown in Figure 3, including a representative SEM image of the raw laser SWNT soot. The raw laser SWNT soot is typically purified using a nitric acid reflux followed by controlled thermal oxidation treatments to maximize purification efficiency.

The MWNTs are synthesized by injection-chemical vapor deposition(CVD) using a cyclopentadienyldicarbonyl iron dimer dissolved in toluene (1). The precursor solution (0.1 M) is injected at controlled flow rates (typically 1-2 L/min) under flowing $Ar_{(g)}$ at 725 °C. The as-produced MWNTs condense onto the quartz substrate outside the furnace and are relatively free of metal catalyst impurities based on thermogravimetric analysis (< 5 % w/w). The CVD reactor set-up is described in the schematic of Figure 4, including a representative SEM image of the raw MWNT soot. The SWNTs and MWNTs can both be processed into "paper" form at any level of purity, which has the potential to form electrical contacts in a photovoltaic device.
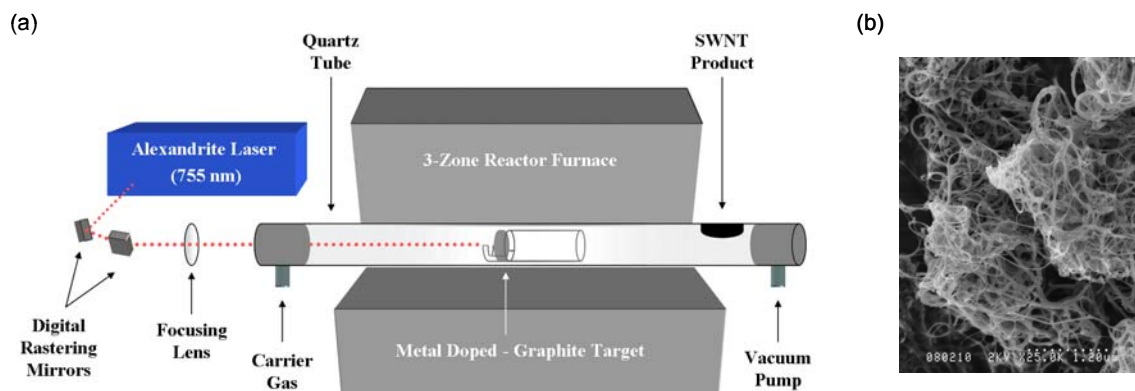
Figure 3. (a) Schematic representation of an Alexandrite Laser Vaporization Reactor for the synthesis of Single Wall Carbon Nanotubes (SWNTs) and (b) scanning electron micrograph (SEM) of raw SWNT soot from this reactor.
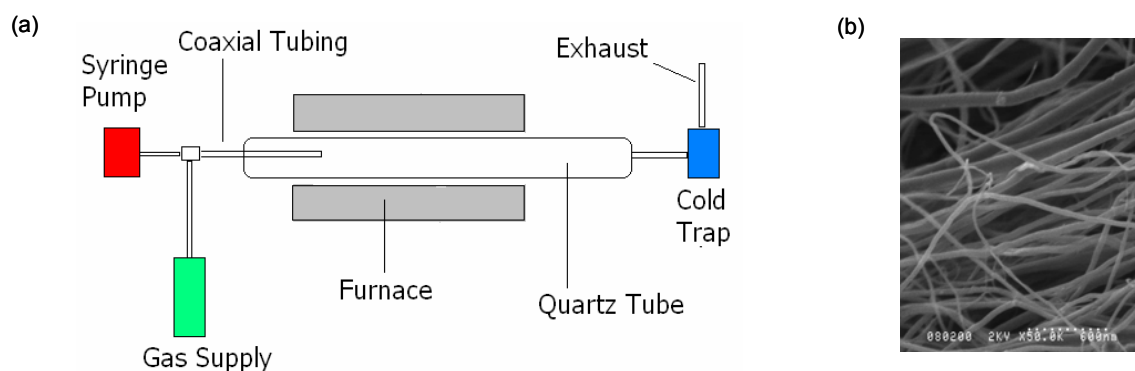
Figure 4. Schematic representation of an Injection Chemical Vapor Deposition Reactor for the synthesis of Multi-Walled Carbon Nanotubes (MWNTs) and (b) SEM of raw MWNT soot from this reactor.

Results & Discussion

Material standardization of CNTs is a critical step towards developing reproducible, high efficiency PV devices. During the synthesis of carbon nanotubes, the by-products are the principal component of the as-produced materials or raw "soot." By-products such as graphitic and amorphous carbon phases, metal catalysts, fullerenes, and carbonaceous coatings on the CNTs may not only dominate the physical characteristics of the raw soot, but they also pose significant challenges in any subsequent purification (19-25). Additionally, the experimental methods used to fabricate SWNTs (i.e. arc-discharge, chemical vapor deposition, and pulsed laser vaporization), produces SWNTs with differing diameter, chirality distributions. Therefore, considerable work is ongoing to develop techniques and methods whereby the types, amount, and morphology of carbon nanotubes can be accurately and precisely quantified (26). Recently, we developed a verified purity assessment method for SWNTs using N,N-dimethylacetamide (DMA) dispersions (17,18). This approach is based on utilizing a calibration curve from a constructed sample set comprising designed mass fractions of purified SWNTs with carbonaceous impurities in the form of nanostructured carbon. Shown in Figure 5a is an example of a constructed sample set using optical absorption spectra for laser-synthesized SWNT-DMA dispersions. The ratio of the $^{S}E_{22}$ and $^{M}E_{11}$ peaks can be used a direct probe to the weight fraction of SWNTs in the carbonaceous portion of the nanotube-containing sample (17,18). This assessment protocol is capable of monitoring the carbonaceous purity of SWNTs from the raw soot through purification treatments to the purified state. Further refinements in this procedure to include other diameter distributions and chemically functionalized species will allow for standardized purity metrics in SWNT assessment.
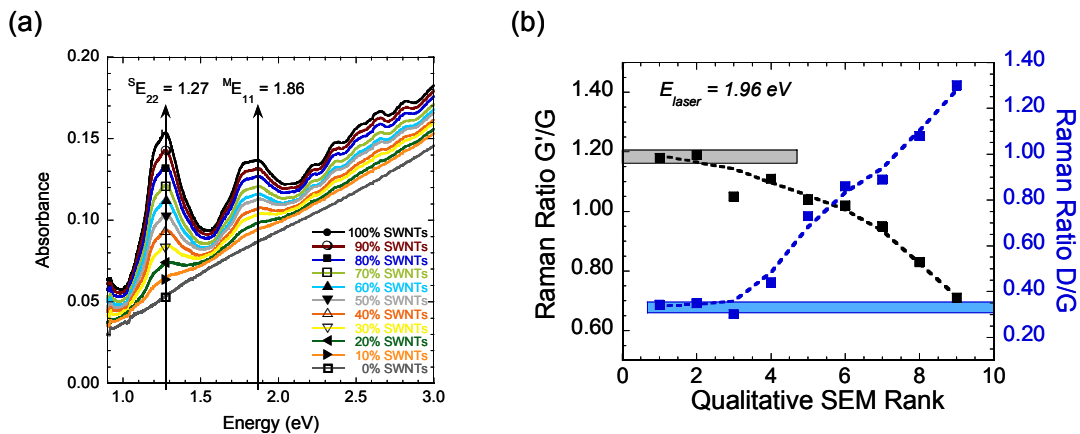
Figure 5. (a) Constructed sample set of laser SWNTs in N,N-dimethylacetamide (DMA) for SWNT purity assessment. (b) Raman ratios of the G'/G and D/G peaks at 1.96 eV excitation for a series of MWNT samples ranked by SEM quality.

Purity assessment of MWNTs is also a sought after research goal, but it is notably more difficult since there are no pronounced spectral features in the optical absorption spectrum that can be directly related to the concentration of the sample (1). Through evaluation of various experimental conditions during the injection-CVD synthesis process, we have identified particular trends which result in the capability for MWNT quality assessment. Based on a series of nine raw MWNT samples which were evaluated by both SEM and Raman spectroscopy (1.96 eV excitation), there exists a trend between ratios of certain Raman peaks with observed material quality. The results are generated from a qualitative SEM ranking where the assessment value ranges between 1 and 9 with the following definitions: 1 - connotes high quality nanotubes in physical structure with no apparent carbonaceous impurities or coatings; and 9 – connotes visual carbonaceous impurities without the presence of nanotube structures. The SEM ranking in conjunction with calculated ratios of the G'/G peaks and D/G peak is shown in Figure 5b. The strong correlation between the calculated data and the qualitative SEM assessment imply that higher G'/G ratios and lower D/G ratios indicate better material quality. These results are consistent with a reduction in carbonaceous impurities or defects which would impact the D/G ratio (1) as it approaches 0.3, and possibly an enhanced resonance effect leading to the increased G'/G ratio in better quality MWNTs converging at a value of ~ 1.2.
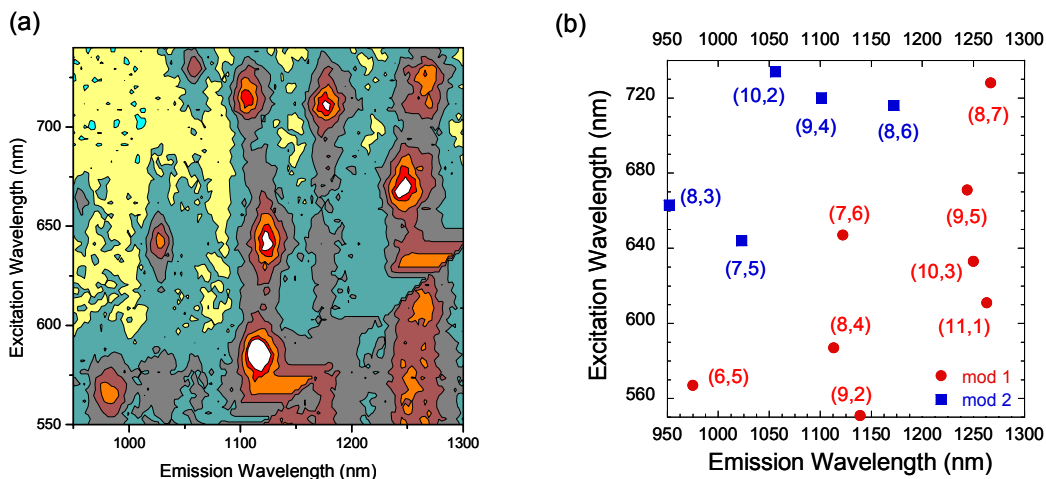
Figure 6. (a) Fluorescence map of raw HiPco SWNTs in 1% w/w SDS-D_2O and (b) SWNT chiral assignments for the semiconducting species present.

Given that developments in purity assessment are establishing material standards for carbon nanotubes, further advancement with respect to SWNT-based PV devices will require control over optical bandgap and electronic-type separations. The recently published "ideal" diode results capitalize on a semiconducting SWNT behaving with a specific bandgap derived from its geometry. Being able to identify the various chiralities of semiconducting species present in a given sample is a critical analysis. Since synthesis techniques produce SWNTs with differing diameter and chirality distributions, there needs to exist methods of quantifying the SWNT chiral concentrations which can enable post-synthesis separations monitoring. The recent discovery of SWNT solution-phase fluorescence spectroscopy represents a viable technique to probe changes in such distributions (27). It should be noted that Raman spectroscopy is currently the method of choice for assessing electronic type separations since only semiconducting SWNTs exhibit near-IR fluorescence transitions (28). Shown in Figure 6a is a typical fluorescence map of raw HiPco SWNTs dispersed in a 1% w/w sodium dodecyl sulfate (SDS)-D_2O dispersion. The optical bandgap of these SWNTs is observed over a wavelength range of 950-1300 nm (~1 - 1.3 eV). Based on the excitation wavelength, chiral designations can be made to determine the diameter and helicity of the SWNTs in a given sample. These assignments are listed in Figure 6b, based on the previously published work (27). Thus, near-IR fluorescence spectroscopy can provide a detailed assessment of the SWNT semiconducting content in a given sample and future work aims at using internal standards to quantify the concentration of semiconducting SWNTs present.

(a)   (b)
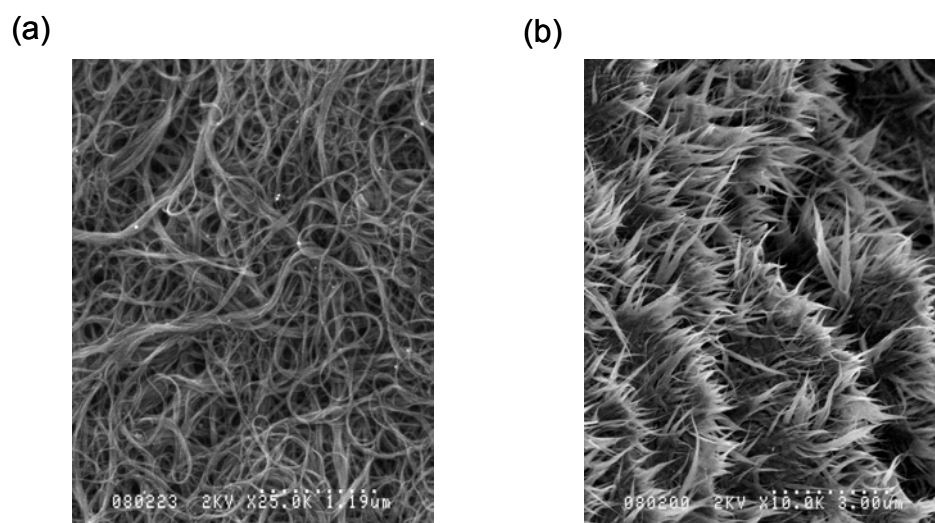
Figure 7. SEM images of (a) normal length purified SWNTs and (b) "as-cut" SWNTs from ultrasonication in a 3:1 mixture of concentrated H_2SO_4 and H_2O_2 for 8 hrs.

Although the high aspect ratio of SWNTs is at times a desirable property, in the case of a SWNT-polymer composite film for PV devices, the SWNT length may need to be controlled. For example, the thickness of the composite should be <<1 μm to optimize hole transport in the polymer, but the average lengths of purified SWNTs can be from 1-10 μm. Therefore, a controlled cutting of the SWNTs will reduce shunting effects in these devices, while maintaining the high electrical conductivity necessary to extract the electrons out of the polymer to the negative electrode. Based on a recent report (29), we have employed a piranha solution (3:1 mixture of concentrated H_2SO_4 and H_2O_2) to chemically cut SWNTs in the presence of ultrasonication. Shown in Figure 7 are SEM images of the (a) purified SWNTs prior to cutting and (b) the "as-cut" sample after 8 hour exposure. The significant number of tip ends, as compared to the full-length entangled purified SWNT sample, is evidence that the nanotubes were cut. Further evidence comes from atomic force microscopy (AFM) analysis which shows that the average lengths in the "as-cut" sample are < 500 nm whereas the purified SWNTs were at least 1- 2 μm long. Incorporation of these "cut" SWNTs into a composite will potentially reduce the observed shunting in typical SWNT-Polymer solar cells.

There are currently many research efforts to develop high efficiency polymeric solar cells which utilize nanomaterial-polymer junctions. The limitation in most of these devices is that the optical bandgap of the polymer is > 2 eV which is not ideal for the solar spectrum (~1.4 eV). Therefore, we have been developing strategies for chemical attachment of chromophores which absorb the lower energy light and can efficiently charge transfer to the polymer matrix. Specifically, the attachment of semiconducting quantum dots (QDs) like CdSe have shown tunable absorption properties, high extinction coefficients, and optimal energy levels for charge transfer to certain conducting polymers (30). With this in mind, we have demonstrated covalent bonding strategies to couple the QDs to SWNTs and a diagram of the aminoethanethiol-linked product is shown in Figure 8a. These QD-SWNT complexes have been incorporated into polymer devices and show improved PV conversion compared to the intrinsic polymer. However, it has been apparent during our work, that significant disruption of the carbon-carbon bonds in the SWNTs from such attachment can decrease the ability to efficiently extract carriers, as observed by the low measured current densities. Therefore, chemical attachment using a noncovalent approach which maintains the structural integrity of the SWNTs has been evaluated. This strategy using a noncovalent linker molecule involving 1-pyrenebutanoic acid succinimidyl ester (PBASE), and the product is shown in Figure 8b. Evaluation of the noncovalent product as a superior attachment means for polymer PV is currently underway, however, spectroscopic data does show an electronic interaction between nanomaterials which would be necessary for optimal performance.
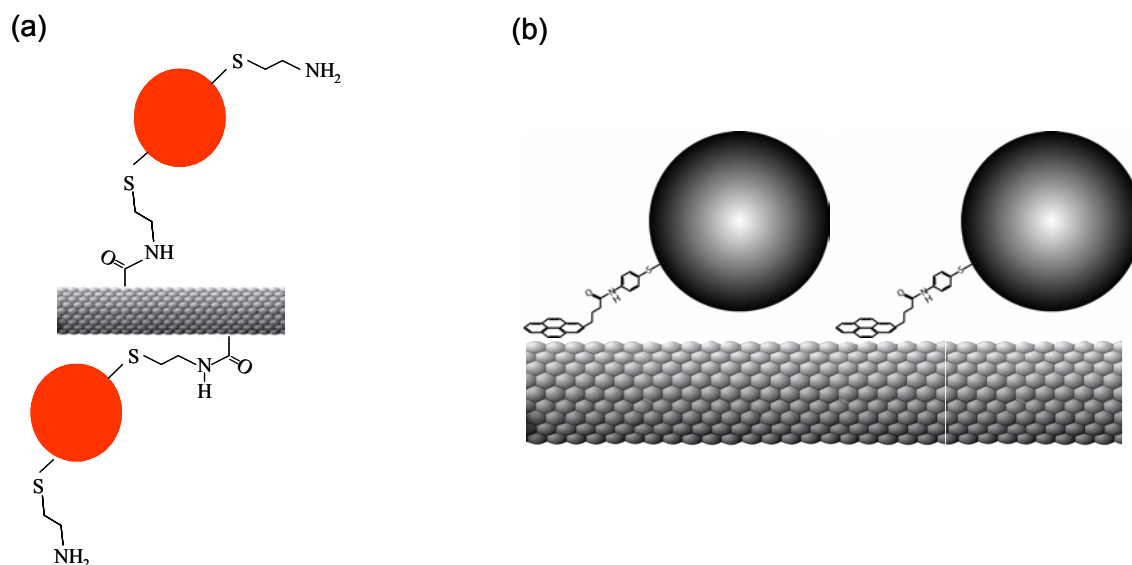
Figure 8. Diagrams showing the chemical attachment of semiconducting quantum dots to SWNTs through (a) covalent bonding with an aminoethanethiol ligand and (b) noncovalent bonding with a pyrene ligand.

Conclusions

The application of carbon nanotubes to space PV is a relatively new, but potentially rewarding area of research based on the extraordinary optical, electrical, and mechanical properties of these materials. Recent developments have shown carbon nanotube diodes to exhibit "ideal" behavior while others have demonstrated utility of carbon-nanotube polymer composites as solar cells. The ongoing success of these materials will be based on the development of material standards revolving around synthesis, purification, and chiral separations. In our recent work, we have investigated laser vaporization synthesis of SWNTs with appropriate purity assessment protocols for SWNT materials. Additionally, the use of injection-CVD to produce high quality MWNT samples has been demonstrated and various experimental conditions have allowed for a MWNT purity assessment based on a Raman ratio analysis. The use of NIR fluorescence spectroscopy to quantitatively assess the semiconducting distribution of SWNTs in a sample will assist in future diameter and chiral separations. Finally, the utility of "cut" SWNTs and complexes involving the chemical attachment of QDs to SWNTs is expected to lead to higher efficiency polymeric solar cells by enhancing charge transfer and optical absorption characteristics.

Acknowledgements

References

(1)   R.P. Raffaelle, B.J. Landi, J.D. Harris, S.G. Bailey, A.F. Hepp, Mater. Sci. Eng. B 116 (2005) 233-243.
(2)   H. Dai, Surf. Sci. 500 (2002) 218-241.
(3)   S. Huang, M. Woodson, R. Smalley, J. Liu, Nano Lett. 4 (2004) 1025-1028.
(4)   http://www.nanotechnologies.qc.ca/projets/hydrogene/images/en/nanotubes_large.jpg.
(5)   J.U. Lee, Appl. Phys. Lett. 87 (2005) 073101.
(6)   A. Thess, R. Lee, P. Nikolaev, H. Dai, P. Petit, J. Robert, C. Xu, Y.H. Lee, S.G. Kim, A. Rinzler, D.T. Colbert, G. Scuseria, D. Tomanek, J.E. Fischer, R. Smalley, Science 273 (1996) 483487.
(7)   S. Berber, Y.-K. Kwon, D. Tomanek, Phys. Rev. Lett. 84 (2000) 4613-4616.
(8)   L.S. Schadler, S.C. Giannaris, P.M. Ajayan, Appl. Phys. Lett. 73 (1998) 3842.
(9)   F. Li, Cheng, H.M.; Bai, S.; Su, G.; Dresselhaus, M.S., Appl. Phys. Lett. 77 (2000) 3161-3163.
(10)   J. Salvetat, G.A.D. Briggs, J. Bonard, R.R. Bacsa, A.J. Kulik, T. Stockli, N.A. Burnham, L. Forro, Phys. Rev. Lett. 82 (1999) 944.
(11)   M. Cinke, J. Li, B. Chen, A. Cassell, L. Delzeit, J. Han, M. Meyyappan, Chem. Phys. Lett. 365 (2002) 69.
(12)   E. Kymakis, G.A.J. Amaratunga, Appl. Phys. Lett. 80 (2002) 112-114.
(13)   B.J. Landi, R.P. Raffaelle, S.L. Castro, S.G. Bailey, Prog. Photovot: Res. Appl. 13 (2005) 1-8.
(14)   T. Guo, P. Nikolaev, A.G. Rinzler, D. Tomanek, D.T. Colbert, R.E. Smalley, J. Phys. Chem. 99 (1995) 10694-10697.
(15)   A.C. Dillon, P.A. Parilla, J.L. Alleman, J.D. Perkins, M.J. Heben, Chem. Phys. Lett. 316 (2000) 13-18.
(16)   E. Munoz, W.K. Maser, A.M. Benito, M.T. Martinez, G.F. de la Fuente, A. Righi, E. Anglaret, J.L. Sauvajol, Synth. Met. 121 (2001) 1193-1194.
(17)   B.J. Landi, H.J. Ruf, C.M. Evans, C.D. Cress, R.P. Raffaelle, J. Phys. Chem. B 109 (2005) 9952-9965.
(18)   B.J. Landi, H.J. Ruf, J.J. Worman, R.P. Raffaelle, J. Phys. Chem. B 108 (2004) 17089-17095.
(19)   I.W. Chiang, B.E. Brinson, R.E. Smalley, J.L. Margrave, R.H. Hauge, J. Phys. Chem. B 105 (2001) 1157-1161.
(20)   I.W. Chiang, B.E. Brinson, A.Y. Huang, P.A. Willis, M.J. Bronikowski, J.L. Margrave, R.E. Smalley, R.H. Hauge, J. Phys. Chem. B 105 (2001) 8297-8301.
(21)   A.C. Dillon, T. Gennett, K.M. Jones, J.L. Alleman, P.A. Parilla, M.J. Heben, Adv. Mater. 11 (1999) 1354-1358.
(22)   A.C. Dillon, T. Gennett, P.A. Parilla, J.L. Alleman, K.M. Jones, M.J. Heben, Mater. Res. Soc. Symp. Proc. 633 (2001) A5.2.1-A5.2.6.
(23)   A.R. Harutyunyan, B.K. Pradhan, J. Chang, G. Chen, P.C. Eklund, J. Phys. Chem. B 106 (2002) 8671-8675.
(24)   J.-M. Moon, K.H. An, Y.H. Lee, Y.S. Park, D.J. Bae, G.-S. Park, J. Phys. Chem. B 105 (2001) 5677-5681.
(25)   K.L. Strong, D.P. Anderson, K. Lafdi, J.N. Kuhn, Carbon 41 (2003) 1477-1488.
(26)   S. Arepalli, P. Nikolaev, O. Gorelik, V.G. Hadjiev, W. Holmes, B. Files, L. Yowell, Carbon 42 (2004) 1783-1791.
(27)   S.M. Bachilo, M.S. Strano, C. Kittrell, R.H. Hauge, R.E. Smalley, R.B. Weisman, Science 298 (2002) 2361.
(28)   G.G. Samsonidze, S.G. Chou, A.P. Santos, V.W. Brar, G. Dresselhaus, M.S. Dresselhaus, A. Selbst, A.K. Swan, M.S. Unlu, B.B. Goldberg, D. Chattopadhyay, S.N. Kim, F. Papadimitrakopoulos, 85 (2004) 1006.
(29)   K. Ziegler, J., Z. Gu, H. Peng, E.L. Flor, R.H. Hauge, R.E. Smalley, J. Am. Chem. Soc. 127 (2005) 1541-1547.
(30)   B.J. Landi, H.J. Ruf, C.M. Evans, S.G. Bailey, S.L. Castro, R.P. Raffaelle, Sol. Ener. Mat. & Sol. Cells 87 (2005) 733-746.